Applied Surface Science 256 (2010) 4462–4467

Contents lists available at ScienceDirect

Applied Surface Science

journal homepage: www.elsevier.com/locate/apsusc

Influence of temperature annealing on optical properties of $SrTiO_3/BaTiO_3$ multilayered films on indium tin oxide

T. Supasai [a], S. Dangtip [b], P. Learngarunsri [b], N. Boonyopakorn [b], A. Wisitsoraat [c], Satreerat K. Hodak [a,d,*]

[a] Department of Physics, Faculty of Science, Chulalongkorn University, Bangkok 10330, Thailand
[b] Department of Physics, and NANOTEC COE at Mahidol University, Faculty of Science, Mahidol University, Bangkok 10400, Thailand
[c] Nanoelectronics and MEMS Laboratory, National Electronics and Computer Technology Center (NECTEC), Thailand 12120
[d] Center of Innovative Nanotechnology, Chulalongkorn University, Bangkok 10330, Thailand

ARTICLE INFO

Article history:
Received 20 August 2009
Received in revised form 20 November 2009
Accepted 22 January 2010
Available online 1 February 2010

PACS:
78.20.Ci

Keywords:
Perovskites
Optical properties
Multilayers
Annealing
Sol–gel

ABSTRACT

We have prepared $SrTiO_3/BaTiO_3$ thin films with multilayered structures deposited on indium tin oxide (ITO) coated glass by a sol–gel deposition and heating at 300–650 °C. The optical properties were obtained by UV–vis spectroscopy. The films show a high transmittance (approximately 85%) in the visible region. The optical band gap of the films is tunable in the 3.64–4.19 eV range by varying the annealing temperature. An abrupt decrease towards the bulk band gap value is observed at annealing temperatures above 600 °C. The multilayered film annealed at 650 ° C exhibited the maximum refractive index of 2.09–1.91 in the 450–750 nm wavelength range. The XRD and AFM results indicate that the films annealed above 600 ° C are substantially more crystalline than the films prepared at lower temperatures which were used to change their optical band gap and complex refractive index to an extent that depended on the annealing temperature.

1. Introduction

Thin films made of high dielectric constant materials based on alkaline earth titanates of $BaTiO_3$ (BTO) and $SrTiO_3$ (STO) have received much attention due to their applications in dynamic random access memories (DRAMs) [1], high dielectric capacitors [2–4], and tunable microwave devices [5]. In addition, due to their large electro-optical coefficient, low optical losses, and excellent optical transparency in the visible region, these materials can be used in optoelectronic devices. An application of these types of films as insulating layer in flat panel displays (FPD) comprising of the layer of metal-electrode/phosphor/insulator/transparent electrode/glass has recently been reported [6,7]. Tunable dielectric response for $BaTiO_3$ and $SrTiO_3$ via an applied electric field is a well established characteristic of these materials. However, the optimum tunability occurs at vastly different temperatures ($\sim$ 4–100 K for $SrTiO_3$[4,8] and $\sim$ 250–400 K for $BaTiO_3$[9,10]). Several approaches have been employed to enhance the tunability of dielectric constant near room temperature. Experiments showed that an increase of the tunability of dielectric constant at room temperature can be achieved through film growth of $Ba_{1-x}Sr_xTiO_3$ compound [3,11,12] and by the use of $SrTiO_3/BaTiO_3$ multilayered thin films [13–16]. These composite films have already been prepared with various deposition techniques such as pulsed laser deposition [4,8,16–19], RF sputtering [12,20], and by sol–gel method [3,13,21]. The dielectric response as well as the structural and optical properties of these perovskite materials depend on the growth conditions, the annealing temperature [22], the type of substrate or buffer layer used [23,24], the thickness [21], and the doping [25]. Xu et al. used a sol–gel technique to prepare polycrystalline $SrTiO_3/BaTiO_3$ multilayered film on $Pt/Ti/SiO_2/Si$ substrate and compared the dielectric response with the uniform $BaTiO_3$ and $SrTiO_3$ films [13]. They found that the dielectric constant of the polycrystalline $SrTiO_3/BaTiO_3$ multilayered films could reach the 400–600 range at 10 kHz while keeping the dielectric loss near that of the uniform films. In another work, epitaxial $SrTiO_3/BaTiO_3$ multilayered films of 8 Åfor each layer prepared by pulsed laser deposition yielded dielectric constants even higher, ranging from 500 to 900 at 10 kHz at room temperature [17]. Moo-Chin Wang's group have found the increase in the dielectric constant of $(SrTiO_3/BaTiO_3)_n$ multilayered thin films grown by RF magnetron sputtering by increasing the number of layers up to 4 [26,27]. Relatively few works dealt with the optical

* Corresponding author at: Department of Physics, Faculty of Science, Chulalongkorn University, Payathai Rd., Bangkok 10330, Thailand.
Tel.: +66 2 218 7557; fax: +66 2 253 1150.
E-mail address: Satreerat.H@Chula.ac.th (S.K. Hodak).

0169-4332/$ – see front matter © 2010 Elsevier B.V. All rights reserved.
doi:10.1016/j.apsusc.2010.01.072

properties of $SrTiO_3/BaTiO_3$ multilayered films despite of much growing interest in these films for device applications [28,29]. In this work, we focused on the effect of the annealing temperature $SrTiO_3/BaTiO_3$ multilayered thin films with different thickness prepared by sol–gel deposition on substrates made of indium tin oxide (ITO) on glass. We found that the optical band gap and complex refractive index of the films can be adjusted by controlling the annealing temperature and the thickness.

2. Experimental details

Glass substrates were cleaned in an ultrasonic bath with acetone, methanol, deionized water and dried with a nitrogen stream. The substrates were then transferred to the deposition chamber. Tin-doped indium oxide (indium tin oxide, ITO) was deposited by rf-magnetron sputtering method under argon plasma to a thickness of 100 nm. The ITO films were post-annealed at 400 °C for 90 min in an argon atmosphere. The typical resistivity of the ITO film was 3×10^{-4} ohm cm with transparency above 90% in the visible region. The raw materials used for the synthesis $BaTiO_3$ and $SrTiO_3$ solution were barium acetate ($Ba(CH_3COO)_2$), strontium acetate ($Sr(CH_3COO)_2$), titanium n-butoxide ($Ti(C_4H_9O)_4$), acetic acid as a solvent and methanol as a stabilizer. Barium acetate and strontium acetate were dissolved in acetic acid at ca. 60 °C with stirring. After homogeneous solutions were obtained, 3.47 ml of pure titanium n-butoxide was added to each solution. The solutions were then diluted by addition of 1.75 ml of methanol. This dilution is necessary to prevent the formation of a precipitate of TiO_2. The deposition of the first layer was done with the Ba solution by spin coating on ITO coated glass at 1000 rpm for 45 s. After the first deposition, the films were preheated on a hot plate at 120 °C for 20 min in order to remove the solvent, then the films were heated at rate of 10 °C/min from 25 °C to the desired annealing temperature which was maintained for 20 min in air atmosphere. The same process was repeated for the second layer using the Sr solution. The maximum annealing temperature was limited at 650 °C to avoid softening and deformation of the glass substrate. The Ba and Sr solutions were spun on silicon (1 0 0) substrates as well for comparison with films on ITO coated glass. The crystal structure of the $SrTiO_3/BaTiO_3$ multilayered thin films were characterized by X-ray diffraction (XRD: Model D8 Bruker diffractrometer) using Cu Kα1 with the wavelength of 1.5406 Å. The surface morphology of the films were examined by atomic force microscopy (AFM: Model Veeco Nanoscope V). The optical transmission and absorbance of the films were recorded using UV–vis spectrometer (JENWAY: Model 6405 UV/Vis), and the optical band gap was calculated from transmittance spectra.

3. Results and discussion

3.1. Structural properties

The film thickness measurements were obtained from the cross-section of scanning electron microscope images. The prepared two layer films (STO/BTO) have quite reproducible 250±20 nm thicknesses. The crystallinity of the films was investigated using X-ray diffraction. Fig. 1(a) shows the XRD patterns of $SrTiO_3/BaTiO_3$ films deposited on ITO coated glass substrate as a function of the annealing temperature which varied in the range of 300–650 °C. There were no BTO and STO characteristic diffraction peaks, nor we observed diffraction peaks from contaminating substances for the films annealed at the 300–550 °C temperature range even in the thicker four-layer films (data not shown). The STO/BTO multilayered films showed distinct crystalline peaks at the annealing temperatures of 600 and 650 °C, as indicated by the appearance of characteristic peaks of BTO and

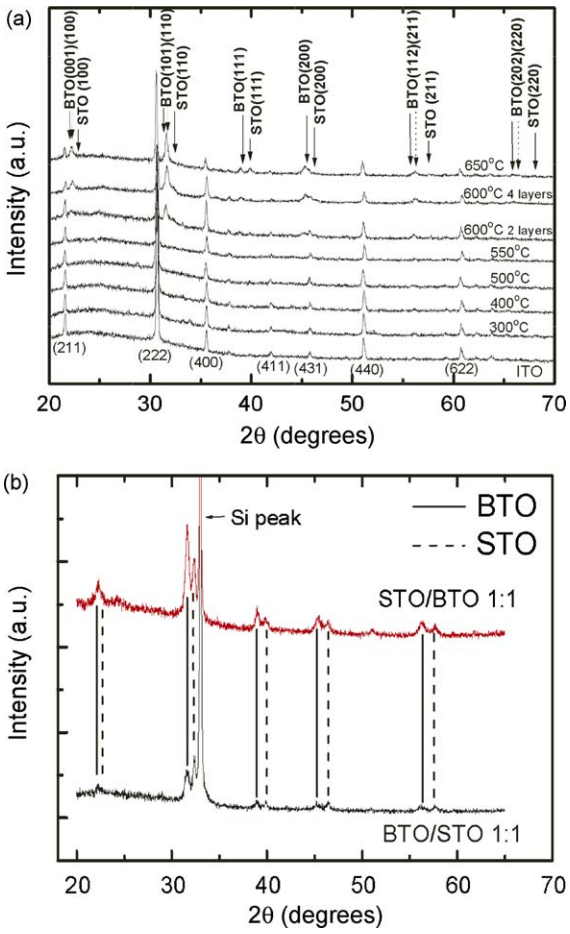

Fig. 1. X-ray diffraction pattern of STO/BTO films annealed at various temperatures (a) on ITO/Glass and (b) on Si (1 0 0) substrate.

STO. The peaks of the X-ray diffraction patterns are sharper and more intense as the annealing temperature increases. However, X-ray spectra of the films annealed at 600 and 650 °C show weak signals suggesting that the films are not well crystallized. With the same annealing temperature of 600 °C, the thicker film (STO/BTO/STO/BTO) showed intense characteristic peaks. Moreover, the full-width at half maximum decreases with the temperature increases. This result is consistent with increased crystallinity of the films at higher annealing temperatures. The average crystallite size t measured in a direction perpendicular to the surface of the specimen was calculated using Scherrer formula as shown in Eq. 1, where B represents a width measured in radians at an intensity equal to half of the maximum intensity, θ_B is the Bragg angle and k is the shape factor of the average crystallite [30]:

$$t = \frac{k\lambda}{B\cos\theta_B} \quad (1)$$

The parameter B is the full width half of the maximum (FWHM) which increases as the crystal size decreases. The calculation was done with $k = 0.94$ by assuming a Gaussian peak shape and a cubic crystal structure. For this analysis, we have chosen the most intense BTO (1 1 1) and STO (1 1 1) peaks which did not overlap with ITO peaks. The crystal sizes of BTO and STO films annealed at 650 °C are 44±4 nm and 37±4 nm, respectively, while for BTO and STO film annealed at 600 °C are approximately 26±5 nm and 14±5 nm, respectively. Clearly, the crystal size of the $SrTiO_3/BaTiO_3$ films increases with increasing annealing temperature. For four layer film (STO/BTO/STO/BTO) annealed at 600 °C, the crystal

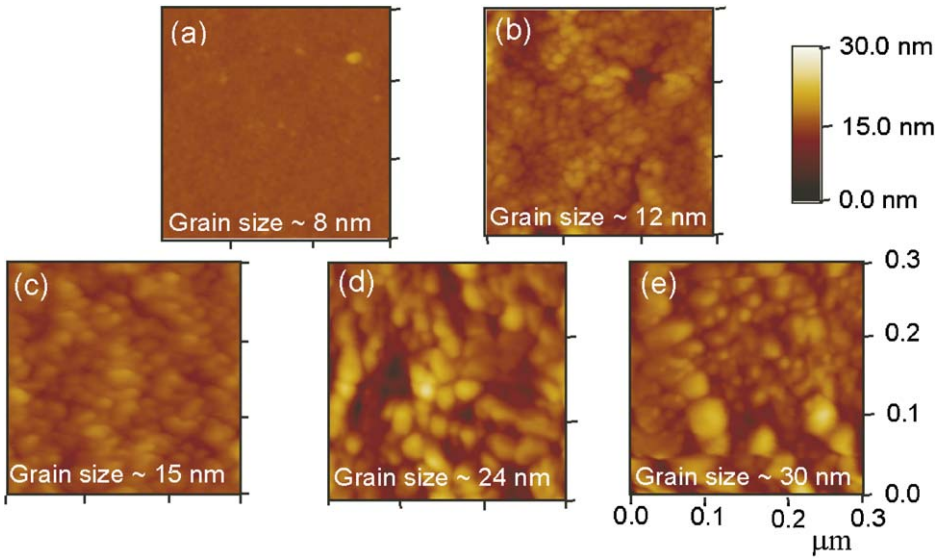

Fig. 2. AFM 2D images (0.3 μm × 0.3 μm) of STO/BTO films deposited on ITO coated glass annealed at various temperatures for 20 min (a) 300 °C, (b) 500 °C, (c) 550 °C, (d) 600 ° C and (e) 650 °C.

sizes of BTO and STO films are 44 ± 4 nm and 24 ± 4 nm, respectively. The crystallite size of BTO is slightly larger than that of STO. This is due to the fact that the BTO solution was deposited on the first layer which was annealed for two times longer than that of the top STO film. We further prove this assumption by inverting the order of the film layer and depositing on Si (1 0 0) substrates. By comparing the X-ray diffraction patterns of STO/BTO and BTO/STO films as presented in Fig. 1(b), we clearly see that the film located in the first layer showed higher and narrower peaks.

The X-ray diffraction patterns of the films annealed at 600 and 650 ° C showed a splitting of the BTO peaks. This suggests that BTO adopted tetragonal structure. Our calculated lattice parameters for BTO were $a = 3.995 \pm 5$ Å and $c = 4.011 \pm 5$ Å while STO structure exhibited a cubic structure with lattice constant of 3.905 ± 5 Å. We did not observe any phase transition and all the films annealed at 600 and 650 ° C showed the same X-ray diffraction patterns. The surface of morphology was investigated by atomic force microscopy (AFM). Fig. 2 presents AFM images of the STO/BTO films as a function of annealing temperature. The grain sizes of the films also increases with increasing annealing temperatures reaching ca. 30 nm at 650 °C. This may result from higher atom mobility with increasing temperature which causes a more effective recrystallization of the material of the films and resulting in larger grains.

3.2. Optical properties

Fig. 3 shows the optical transmission spectra of STO/BTO films annealed at various temperatures in the 200–800 nm wavelength range. The transmission spectra of glass and ITO/glass are shown in the same figure for comparison. All the films annealed at high temperatures were transparent and exhibited optical transmittance of ca. ~85% in the visible region. The oscillations in the transmittance curve due to interference have low depths of modulation indicating inhomogeneity of the films across the light beam. Overall, the films annealed at higher temperatures displayed lower transmittance. The thickness d of the film can be determined using the envelope method according to Swanepoel [31] where $n(\lambda_1)$ and $n(\lambda_2)$ are refractive indices of two adjacent maxima or minima at wavelengths λ_1 and λ_2, respectively:

$$d = \frac{\lambda_1 \lambda_2}{2[n(\lambda_1)\lambda_2 - n(\lambda_2)\lambda_1]} \quad (2)$$

The resulting film thickness of 250±20 nm calculated from Eq. 2 is consistent with the cross-sectional image from scanning electron microscopy. From the optical transmission spectra, the absorption coefficient (α) of the films was determined from the equation:

$$\alpha = \frac{1}{d} \ln\left(\frac{1}{T}\right) \quad (3)$$

where T is the normalized transmittance and d is thickness of the films [32]. All the films showed a sharp absorption onset in the near-UV region. The absorption edge of the films shifts to longer wavelengths as the annealing temperature increases. It is known that exciton–phonon coupling or dynamic disorder is the main factor contributing to absorption edge broadening for crystalline materials [33]. In amorphous materials, imperfections and disorder bring additional broadening due to static disorder. In the films of smallest grains changes in Urbach-type absorption tail manifest the static inhomogeneity due to the presence of localized states within the gap and maybe quantified by the steepness of the band edge [33] which can be estimated from the slope of the plot of α^2 versus $h\nu$ at the beginning of band-to-band absorption [34]. The band edge steepness of our film increased with increasing the annealing temperature suggesting that the density of localized

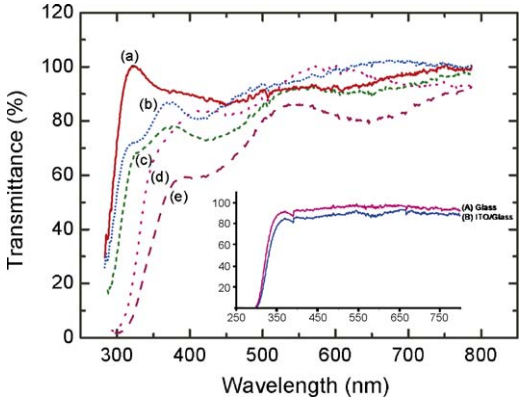

Fig. 3. Transmittance spectra of STO/BTO films annealed at various temperatures for 20 min: (a) 300 °C, (b) 500 °C, (c) 550 °C, (d) 600 ° C and (e) 650 °C; (A) glass and (B) ITO/glass.

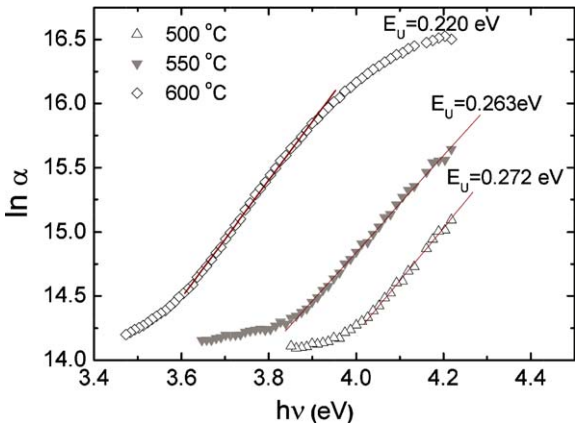

Fig. 4. Determination of the Urbach energy for STO/BTO films annealed at 500, 550 and 600 ° C from the absorption coefficient.

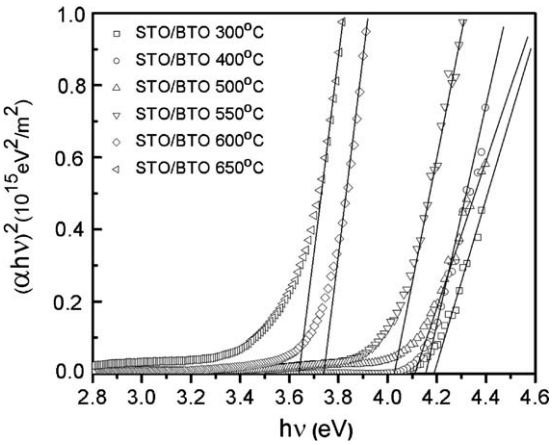

Fig. 5. Plot of $(\alpha h\nu)^2$ versus $h\nu$ for STO/BTO films annealed at various temperatures.

states decrease with heating temperature. A more quantitative measurement of the band edge characteristic can be obtained from so-called Urbach rule [35]. In general, an exponentially increasing absorption edge can be seen in various types of materials:

$$\alpha = \alpha_0 \exp\left(\frac{\sigma(h\nu - E_0)}{kT}\right) = \alpha_0 \exp\left(\frac{h\nu - E_0}{E_U}\right) \quad (4)$$

where and α_0 and E_0 are the Urbach bundle convergence point coordinates, E_U is the absorption edge energy width interpreted as the width of the tails of localized states in the band gap and σ is the steepness parameter, k is the Boltzmann constant and T is the temperature. Fig. 4 shows the plot of lnα versus $h\nu$ at different annealing temperatures. The calculated Urbach energy which is inverse to the absorption edge slope value ($E_U = (kT/\sigma)$) for STO/BTO films annealed at 500, 550 and 600 °C, respectively, are 0.272, 0.263 and 0.220 eV, respectively.

As the annealing temperature increases, larger grains are formed which brings an increased band edge steepness. This may be explained by the reduction of the surface to volume ratio as crystals grow larger since the localized states most likely arise from surface states.

The Tauc relation between the absorption coefficient and direct and indirect band gap energies (E_g) are given by [32,36]:

$$(\alpha h\nu)^2 \sim (h\nu - E_g), \quad (5)$$

and

$$(\alpha h\nu)^{1/2} \sim (h\nu - E_g), \quad (6)$$

for allowed direct transitions and indirect transitions, respectively, where $h\nu$ is the energy of the incident photon. We plotted $(\alpha h\nu)^n$ ($n = 2$ for direct transition and $n = 1/2$ for indirect transition) versus $h\nu$, and obtained E_g by extrapolating the linear portion of the plot to zero frequency. We found that the best fit to a straight line was obtained for $n = 2$ indicating that a direct allowed transition occurs at Γ point in the Brillouin zone from the valence band maximum to the conduction band minimum. Fig. 5 shows the plot of $(\alpha h\nu)^2$ as a function of $h\nu$ at various annealing temperatures. The same absorption region has been used to evaluate optical band gap [37,38]. Fig. 6 shows the band gap energy versus annealing temperatures. For the films annealed at lower temperatures (300, 400, 500 and 550 °C), the value of the energy gaps gradually decrease with annealing temperature in the range of 4.19–4.03 eV. An abrupt decrease towards the bulk band gap value is observed for the films annealed above 600 ° C yielding the energy gap in the 3.64–3.74 eV range. The experimental direct and indirect band gap energies for BTO are 3.6 and 3.2 eV, respectively [39], while those for STO are 3.75 and 3.25 eV, respectively [40,41]. The band gap of the amorphous phase is about 0.3–0.5 eV larger than that of the crystalline phase [39–41]. The abrupt decrease of energy gap from around 4 to 3.74 eV is consistent with a change in the structure of the films from amorphous to crystalline phase. The results of the energy gap are in agreement with the XRD results that show a more crystalline phase obtained when the films annealed above 600 °C. Similar change in energy gap has been observed for sol–gel derived $BaTiO_3$[7] and $SrTiO_3$ films [21]. We further investigated the thickness effect of optical band gap by depositing four layers films (STO/BTO/STO/BTO) on ITO coated glass. For the same annealing temperature, the thicker films exhibited a reduction in the energy gap which is similar to that shown in Fig. 6. The crystallinity and the grain size of the films increase with the film thickness resulting in a decrease of the energy band gap. The shift of optical band gap energy can be also explained in terms of quantum-size effect in which the films with large crystallites will have red-shifted absorption onsets. By way of comparison, we used the quantum confinement prediction for energy gap [42].

$$E_g(r) = E_g(bulk) + \frac{2\pi^2\hbar^2}{r^2}\left(\frac{1}{|m_e|} + \frac{1}{|m_h|}\right) \quad (7)$$

$$E_g(r) = E_g(bulk) + \frac{2\pi^2\hbar^2}{r^2\mu} \quad (8)$$

where m_e, m_h, μ, r are the effective mass of electron, the effective mass of hole, the reduced mass and the diameter of nanoparticle,

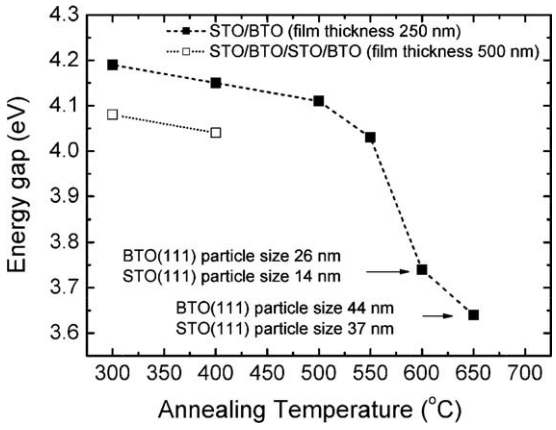

Fig. 6. Temperature and thickness dependence of the band gap energy for STO/BTO multilayered films.

respectively. Normally, if the particle size is smaller than the corresponding DeBroglie wavelength, the size quantization effects can be observed in the band gap. The theoretical calculated DeBroglie wavelength for BTO and STO is about 15 nm, $a_B = (4\pi\varepsilon_0\varepsilon_r\hbar^2)/\mu e^2$ where ε_r is the dielectric constant. Fig. 7 shows a comparison of the theory of quantum confinement model along with the experiment values for the allowed direct and phonon assisted indirect transitions. In the calculation for BTO, we substituted m_e for $0.81m_o$ ($\Gamma\rightarrow$ R direction) and m_h for $-2.78m_o$ (R$\rightarrow$ X direction) for indirect transitions (μ=$0.62m_o$), where m_o is the mass of a free electron equal to 9.11×10^{-31} kg [42,43]. The resulting values of direct band gap energies are larger than those of indirect band gap energies. As the particle size gets larger, the band gap energies approach the bulk values. For smaller crystallite size, there is a shift in band gap from the theoretical curve for both transitions. This is because the values for the effective mass of electron and the effective mass of hole used in our calculation were obtained from bulk assumption using the first principle calculation [43]. A better agreement between our data and the theory can be obtained by adjusting the reduced mass. Such procedure leads to a reduced mass of μ=$0.03m_o$ which would be consistent with band curvatures that are significantly larger than the bulk predictions. One has to note that the band discontinuities are not true infinite potential barriers which softens the confinement of the carriers and may also cause a deviation between the theory and our data. The shift of the energy band gap to the higher energies with decreasing in particle size is caused by destruction of the excitons [44].

We now turn our attention to the optical absorption. Our films showed a sharp absorption near UV region but not in the visible region. In the region of medium and weak absorption, $\alpha \neq 0$ the complex refractive index ($\tilde{n} = n - ik$, where n is the refractive index and k is the extinction coefficient) can be obtained by [31]:

$$n(\lambda) = [N + (N^2 - n_s^2)^{1/2}]^{1/2} \tag{9}$$

where

$$N = \frac{(n_s^2 + 1)}{2} + 2n_s\frac{(T_{\max} - T_{\min})}{T_{\max}T_{\min}} \tag{10}$$

where n_s is the refractive index of ITO/glass substrate, T_{max} and T_{min} are the maximum and minimum transmittances at the same wavelength in the envelop curves, respectively.

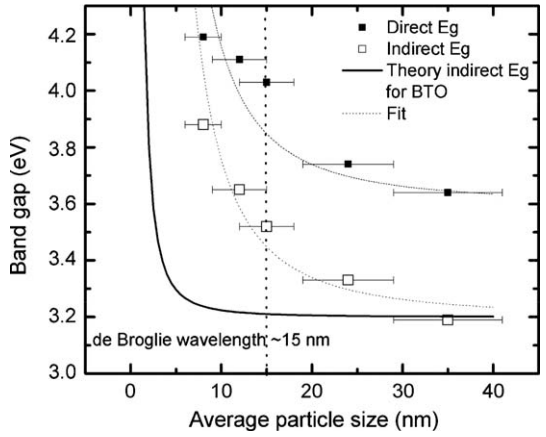

Fig. 7. Direct and indirect band gap energies versus the average particle size. The solid line is a prediction by quantum size effect. The dashed lines are the prediction of the quantum size effect with adjustable effective mass.

The extinction coefficient k, the absorption coefficient α, and the thickness d are related by the following equations [31]:

$$k = \frac{\alpha\lambda}{4\pi} \tag{11}$$

$$\alpha = \frac{1}{d}\ln\frac{(n-1)(n_s-n)[1+(T_{\max}/T_{\min})^{1/2}]}{(n+1)(n_s+n)[1-(T_{\max}/T_{\min})^{1/2}]} \tag{12}$$

Fig. 8 shows the variation of the dispersion curve of the films with annealing temperature. The refractive index and the extinction coefficient decrease with the wavelength following a typical shape of dispersion curve near an electronic interband transition, rising rapidly toward shorter wavelength [45]. The refractive index increases with increasing annealing temperature. The refractive index of perovskite thin films is known to proportional to their electronic polarization per unit volume which is inversely proportional to distance between atomic planes. This result can be explained by an increase in the density of the film due to better packing and increased crystallinity. The large increase in refractive index and strain relaxation following crystallization obtained for the films annealed at temperature 650 ° C is due to crystallization of the perovskite phase. For comparison with bulk STO (n = 2.30–2.65) [46] and BTO ($n \sim 2.3$) [47] or well crystallized STO (n = 2.15–2.35) [48] and BTO thin films (n = 2.15–2.55) [49], the refractive index of our films is lower. This suggests that crystalline structure of our multilayer films leads to a relatively low density [46–49]. The extinction coefficient of our films is less than 0.05 in the 450–750 nm wavelength range indicating low optical losses with the film annealed at 650 ° C exhibiting the lowest loss.

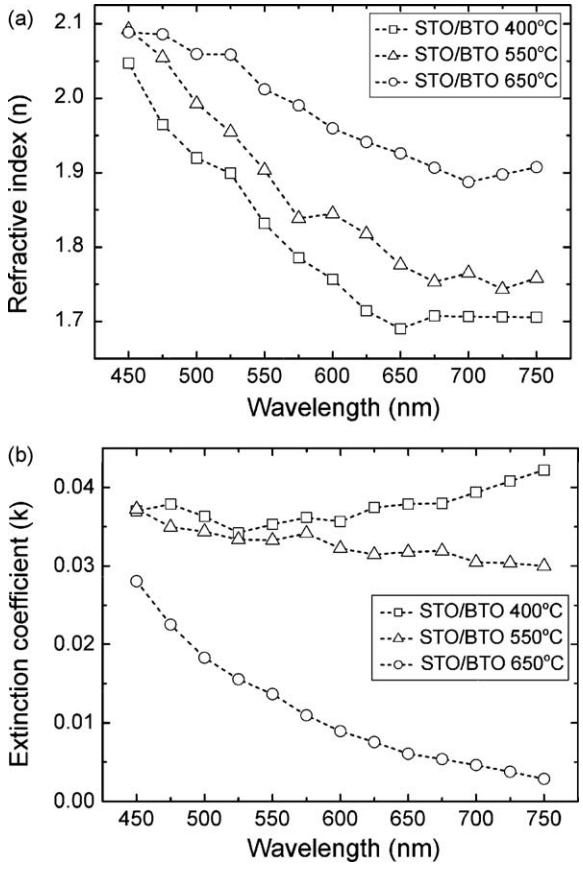

Fig. 8. The variation of (a) refractive index, n and (b) extinction coefficient, k of the films as a function of wavelength.

4. Conclusions

Crystalline $SrTiO_3/BaTiO_3$ multilayered thin films have been prepared on ITO coated on glass by a sol–gel spin coating technique. The structural and optical properties of the films were studied. Our results indicate that the films annealed above 600 ° C show more pronounced crystallinity with large grain size. As the grain decreases, the localized states increase leading to broadening in the absorbance. Tunable band gaps can be obtained by varying annealing temperatures and the film thickness. The variation of the band gap energy upon the particle size follows from quantum confinement effects with somehow smaller carrier-effective masses. The optical band gap of the film annealed at 650 ° C approach the bulk value.

Acknowledgements

The authors would like to thank Mr. Manop Tirarattanasompot for the help in the X-ray measurements. Miss Thidarat Supasai would like to thanks Thailand Graduate Institute of Science and Technology (TGIST) for supporting her Ph.D. study. Authors would like to thank the Thailand Research Fund (TRF), the Thailand Toray Science Foundation (TTSF) and Center of Innovative Nanotechnology (CIN) for financial support. Also, this work was supported by Research Funds from the Faculty of Science, Chulalongkorn University (A1B1), the Thai Government Stimulus Package 2 (TKK2555), under the Project for Establishment of Comprehensive Center for Innovative Food, Health Products and Agriculture and Chulalongkorn University Centenary Academic Development Project. We also thank Dr. Jose H. Hodak for valuable discussions about sol–gel process.

References

[1] M.H. Yeh, Y.C. Liu, K.S. Liu, I.N. Lin, J.Y.M. Leeb, H.F. Cheng, J. Appl. Phys. 74 (3) (1993) 2143.
[2] R. Thomas, D.C. Dube, M.N. Kamalasananb, S. Chandrab, Thin Solid Films 346 (1999) 212.
[3] K.V. Saravanan, K. Sudheendran, M.G. Krishna, K.C. James Raju, K. Anil, Bhatnagar, Mater. Chem. Phys. 105 (2007) 426.
[4] S.K. Hodak, C.T. Rogers, Microelectron. Eng. 85 (2008) 444.
[5] D. Galt, J.C. Price, J.A. Bealle, R.H. Ono, Appl. Phys. Lett. 63 (22) (1993) 3078.
[6] X. Ouyang, A.H. Kitai, T. Xiao, J. Appl. Phys. 79 (6) (1996) 3229.
[7] H.X. Zhang, C.H. Kam, Y. Zhou, X.Q. Han, Y.L. Lam, Y.C. Chan, K. Pita, Mater. Chem. Phys. 63 (2000) 174.
[8] M.J. Dalberth, R.E. Stauber, J.C. Price, C.T. Rogers, Appl. Phys. Lett. 72 (1998) 507.
[9] Y. Guo, K. Suzuki, K. Nishizawa, T. Miki, K. Kato, J. Cryst. Growth 284 (2005) 190.
[10] S. Madeswaran, N.V. Giridharan, R. Varatharajan, G. Ravi, R. Jayavel, J. Cryst. Growth 266 (2004) 481.
[11] I. Aulika, J. Pokorny, V. Zauls, K. Kundzins, M. Rutkis, J. Petzelt, Opt. Mater. 30 (2008) 1017.
[12] B. Panda, A. Dhar, G.D. Nigam, D. Bhattacharya, S.K. Ray, Thin Solid Films 332 (1998) 46.
[13] R. Xu, M. Shen, S. Ge, Z. Gan, W. Cao, Thin Solid Films 406 (2002) 113.
[14] C.S. His, F.Y. Shiao, N.C. Wu, M.C. Wang, Solid State Commun. 125 (2003) 633.
[15] D. Hu, M. Shen, W. Cao, Microelectron. Eng. 83 (2006) 553.
[16] G. Koebernik, W. Haessler, R. Pantou, F. Weiss, Thin Solid Films 449 (2004) 80.
[17] H. Tabata, H. Tanka, T. Kawai, Appl. Phys. Lett. 65 (1994) 1970.
[18] A. Visinoiu, R. Scholz, S. Chattopadhyay, M. Alexe, D. Hesse, Jpn. J. Appl. Phys. 41 (2002) 6633.
[19] J. Hiltunen, J. Lappalainen, J. Puustinen, V. Lantto, H.L. Tuller, Opt. Express 16 (11) (2008) 8219.
[20] A. Ianculescu, M. Gartner, B. Despax, V. Bley, Th. Lebey, R. Gavrila, M. Modreanu, Appl. Surf. Sci. 253 (2006) 344.
[21] D. Bao, X. Yao, N. Wakiya, K. Shinozaki, N. Mizutani, Appl. Phys. Lett. 79 (23) (2001) 3767.
[22] M.N. Kamalasanan, N. Deepak Kumar, S. Chandra, J. Appl. Phys. 76 (8) (1994) 4603.
[23] Y.C. Liang, Y.C. Liang, Scr. Mater. 61 (2009) 117.
[24] H.N. Tsai, Y.C. Liangb, H.Y. Lee, J. Cryst. Growth 284 (2005) 65.
[25] A.Y. Fasasi, M. Maaza, E.G. Rohwer, D. Knoessen, C. Theron, A. Leitch, U. Buttner, Thin Solid Films 516 (2008) 6226.
[26] C.S. Hsi, F.Y. Shiao, N.C. Wu, M.C. Wang, Solid State Commun. 125 (2003) 633.
[27] H.H. Huang, F.Y. Hsiao, N.C. Wu, M.C. Wang, J. Non-Cryst. Solids 351 (2005) 3809.
[28] K. Ruan, X. Chen, T. Liang, G. Wu, D. Bao, J. Appl. Phys. 103 (2008) 074101.
[29] E. Bruno, M.P. De Santo, M. Castriota, S. Marino, G. Strangi, E. Cazzanelli, N. Scaramuzza, J. Appl. Phys. 103 (2008) 064103.
[30] B.D. Cullity, Elements of X-ray Diffraction, Addison-Wesley Publishing Company, Inc., USA, 1978.
[31] R.S. Swanepoel, J. Phys. E.: Sci. Instrum. 16 (1983) 1214.
[32] J.C. Tauc, Optical Properties of Solids, North-Holland, Amsterdam, 1972.
[33] A. Dejneka, A. Churpita, Z. Hubicka, V. Trepakov, Z. Potucek, L. Jastrabik, G. Suchaneck, G. Gerlach, J. Nanosci. Nanotechnol. 9 (2009) 4094.
[34] H. Mertin, R. Esen, J. Cryst. Growth 258 (2003) 141.
[35] F. Urbach, Phys. Rev. 92 (1953) 1324.
[36] J. Tauc, A. Menth, J. Non-Cryst. Solids 8–10 (1972) 569.
[37] J. Wang, J. Xiang, S. Duo, W. Li, M. Li, L. Bai, J. Mater. Sci: Mater. Electr. 20 (2009) 319.
[38] H. Li, Y. Zhang, J. Wen, S. Yang, D. Mo, C.H. Cheng, Y. Xu, J.D. Mackenzie, Jpn. J. Appl. Phys. 39 (2000) 1180.
[39] A. Onton, V. Marrello, G. Lucovsky, F.L. Galeener, AIP Conf. Proc. No. 31, AIP, New York, 1976.
[40] M. Cardona, Phys. Rev. 140A (1965) 651.
[41] K. Van Benthem, C. Elsasser, R.H. French, J. Appl. Phys. 90 (12) (2001) 6156.
[42] K. Suzuki, K. Kijima, Jpn. J. Appl. Phys. 44 (4A) (2005) 2081.
[43] Y.N. Xu, W.Y. Ching, R.H. French, Ferroelectrics 111 (1990) 23.
[44] V.A. Trepakov, Z. Potucek, M.V. Makarova, A. Dejneka, P. Sazama, L. Jastrabik, Z. Bryknar, J. Phys.: Condens. Matter 21 (2009) 375303.
[45] M. Wohlecke, V. Marrello, A. Onton, J. Appl. Phys. 48 (1977) 1748.
[46] M. Cardona, Phys. Rev. 140 (1965) 651.
[47] S.H. Wemple, J. Chem. Phys. 67 (1977) 2151.
[48] T. Hubert, U. Beck, H. Kleinke, J. Non-Cryst. Solids 196 (1996) 150.
[49] W.F. Zhang, Y.B. Huang, M.S. Zhang, Z.G. Liu, Appl. Phys. Lett. 76 (2000) 1003.